COO-1428-237

MASTER

Double-Regge Pole Analysis of $\pi^+ p \to \pi^+ f^0 p$ at 13.1 GeV/c*

J. A. Gaidos, C. R. Ezell, J. W. Lamsa and R. B. Willmann

Physics Department

Purdue University

[illegible], Indiana 47907

LEGAL NOTICE

This report was prepared as an account of work sponsored by the United States Government. Neither the United States nor the United States Atomic Energy Commission, nor any of their employees, nor any of their contractors, subcontractors, or their employees, makes any warranty, express or implied, or assumes any legal liability or responsibility for the accuracy, completeness or usefulness of any information, apparatus, product or process disclosed, or represents that its use would not infringe privately owned rights.

ABSTRACT

A double-Regge model consistent with duality is applied to the reaction $\pi^+ p \to \pi^+ f^0 p$ at 13.1 GeV/c. The diffractively produced πf^0 system is well described by two amplitudes involving Pomeranchuk/A_2 and Pomeranchuk/f^0 exchanges.

*Work supported in part by the U.S. Atomic Energy Commission.

[illegible] IS UNLIMITED

DISCLAIMER

This report was prepared as an account of work sponsored by an agency of the United States Government. Neither the United States Government nor any agency Thereof, nor any of their employees, makes any warranty, express or implied, or assumes any legal liability or responsibility for the accuracy, completeness, or usefulness of any information, apparatus, product, or process disclosed, or represents that its use would not infringe privately owned rights. Reference herein to any specific commercial product, process, or service by trade name, trademark, manufacturer, or otherwise does not necessarily constitute or imply its endorsement, recommendation, or favoring by the United States Government or any agency thereof. The views and opinions of authors expressed herein do not necessarily state or reflect those of the United States Government or any agency thereof.

DISCLAIMER

Portions of this document may be illegible in electronic image products. Images are produced from the best available original document.

1. Introduction

The reactions (a) $\pi^+p \to \pi^+\rho^o p$, (b) $\pi^+p \to \pi^+\pi^-\Delta^{++}$ and (c) $\pi^+p \to \pi^+f^o p$ are the most abundantly produced three body final states in the four-constraint class at 13.1 GeV/c incident beam momentum. These channels [illegible]stically low meson-meson and baryon-baryon four-momentum transfers and can be described by peripheral scattering amplitudes. Discussions of processes (a) [1] and (b) [2] have been given previously in terms of a simple double-Regge model which is consistent with duality. We present here a consideration of reaction (c) within this model and emphasize certain similarities and differences which occur when compared with (a) and (b).

A description of the bubble chamber exposure and data analysis is given in reference (1) where there also appears a graph of the uncut $\pi^+\pi^+\pi^-$ mass spectrum with the A_1 and A_3 enhancements above the $\pi\rho$ and πf^o thresholds respectively.

2. Data Selection

The f^o was selected by requiring $m_{\pi^+\pi^-} = 1.26 \pm 0.1$ GeV; in 5% of the selections both $\pi^+\pi^-$ combinations fell within the f^o mass band. For these cases the combination with invariant mass nearer 1.26 GeV was chosen. In order to avoid the effects of a Δ^{++} contamination, the π^+p invariant mass was restricted to values greater than 1.6 GeV. This cut was chosen lower than the minimum 2.0 GeV in reaction (a) in order to increase the statistical size of the sample. There were no apparent effects attributable to a Δ^{++} influence with this selection. With these rough cuts, the background under the f^o may be as high as 50%. This sample contains 1075 events.

The peripheral nature of reaction (c) is shown in the c.m. longitudinal momentum distributions of the p, f^o and π^+ given in fig. 1, where the sharp

backward peak in the q_L^p spectrum contrasts with the double peaked structures in the $q_L^{f^o}$ and q_L^{π} plots. We interpret these distributions as evidence for diffraction scattering; the sharp backward peak in q_L^p is indicative of diffractive scattering off of the proton and the forward peak in q_L^{π} similarliy is suggestive of diffractive scattering off of the incident pion. The forward peak in $q_L^{f^o}$ is associated with the backward structure in q_L^p; the central enhancement in $q_L^{f^o}$ is associated with the forward peak in q_L^{π}.

In order to separate the contributions of the two diffractive mechanisms, a division of the data was made at $q_L^p = -2.0$ GeV/c; those events with $q_L^p < -2.0$ GeV/c are regarded as proton diffractive, whereas the events with $q_L^p > -2.0$ GeV/c are considered pion diffractive. The four-momentum transfers squared, $t_{\pi\pi}$ and $t_{\pi f}$ for the proton diffractive events were observed to be peaked towards low values with only sparsely populated tails; the cut-offs listed in table 1 were made at points suggested by the data to remove the tails. This same proceedure was followed for the pion diffractive events, with the difference that only t_{pp} was found to be peaked towards small values. This contrasts with the situation in reaction (a) where $t_{p\rho^o}$ was observed to be skewed towards low values simultaneously with t_{pp}. This difference could have been anticipated from fig. 1-b, where the non-forward (hatched) peak in $q_L^{f^o}$ is centered roughly at 0.0 GeV/c, whereas for reaction (a), the corresponding q_L^{ρ} peak occurs at approximately -1.0 GeV/c. Thus, in the pion diffractive events of reaction (a), the q_L^p and q_L^{ρ} distributions are skewed backwards and overlap strongly in values; whereas in reaction (c) only q_L^p is skewed backwards. The accepted kinematical range of the pion diffractive events is also listed in Table 1.

Of the initial 1075 events sample, 485 events fall in the proton diffractive catagory of which 463 are within the limits of Table 1: of the 590 pion diffractive events, 235 are within the cut region.

The cut sample is indicated by hatching in fig. 1, where the correlated disposition of the data suggests that the major portion of reaction (c) can be described by a double peripheral model. We also observe that the

separation of diffractive vertices is essentially unambiguous; there is no evidence for double diffraction.

The four momentum transfers to the diffractive vertices, t_{pp} and $t_{\pi\pi}$ are shown in fig. 2; the line of slope 8.0 $(GeV/c)^{-2}$ drawn through the proton diffractive data is characteristic of elastic πp scattering and the same paramenterization was employed in reaction (a). The slope of 5.5 $(GeV/c)^{-2}$ for the pion diffractive vertex is similar to the values used in reactions (a) and (b).

3. Double-Regge Model

The diagrams corresponding to the amplitudes used to parameterize the data are shown in fig. 3. The diffractive vertices are described by an exponential dependence upon the four-momentum transfers squared, $\exp(8t_{pp})$ and $\exp(5.5_{\pi\pi})$ respectively for the proton diffractive and pion diffractive cases, and coupled to the Pomeranchuk trajectory.

Internal vertices are taken as constants; in particular, no dependence upon the Toller angle is assumed. The nondiffractive vertices are described by a simple pole term of the form $R_a(t) = \beta_a(t)\alpha_a(t)[1 - \tau e^{(-i\pi\alpha_a(t))}]/\Gamma(1+\alpha_a(t))\sin[\pi\alpha_a(t)]$ where a designates the exchange trajectory, $\alpha_a(t)$ is the trajectory, function, taken as the linear form $\alpha_a(t) = J_a - M_a^2 + \alpha'_a(0)\cdot t$, with J_a and M_a the usual particle spin and mass. The signature factor is τ and the values $\alpha_{Pom.} = 1.0$ and $\alpha'_a(o) = 1.0\ (GeV/c)^{-2}$ were assumed throughout. The $\beta_a(t)$ residue factor in $R_a(t)$ was taken as a constant for all three diagrams in fig. 3, and modifications due to spin effects were ignored.

The linear $\alpha_a(t)$ factor is introduced into $R_a(t)$ to cancel the unwanted pole at $\alpha_a(t) = 0$, which would occur in the exchange of the f^o and A_2 trajectories; this factor is not included for π exchange which has no zero.

With the notation A(a[b]) denoting the amplitude for Pomeranchuk coupling to the diffractive [b] vertex and Reggeized (a) exchange to the non-diffractive

vertex, the amplitude corresponding to the diagram in fig. 2-a is then

$$A(f^o[p]) = N(f^o[p])R_{f^o}(t_{\pi\pi})(s_{\pi f^o}/s_o)^{\alpha_{f^o}(t_{\pi\pi})}(s_{f^o p}/s_o)^{\alpha Pom.}\exp(8t_{pp})$$

where $s_o = 1.0\ (GeV/c)^2$.

Calculations of the diagrams illustrated in fig. 3 were carried out using the Monte-Carlo phase space program FOWL [3]. The distributions presented in the following are not all independent and are given to illustrate the overall picture for this type of representation of the data.

Determining the normalization constants $N(f^o[p])$, $N(\pi, [p])$, and $N(A_2[p])$ will form the crux of the following section.

4. Diffractive Proton Vertex

The scatter plot of $-t_{\pi f^o}$ versus $-t_{\pi\pi}$ given in fig. 4-a exhibits a clustering of points along each axis with a predominance of simultaneously low values of the four-momentum transfers. Diagrams 3-a and 3-b yield distributions peaked towards small values of $t_{\pi\pi}$ and $t_{\pi f}$ respectively, but neither diagram is capable of completely describing the reaction. Moreover, there is an area of strong overlap between the two diagrams making the determination of the normalization constants non-trivial. The range and relative strength of influence of the different amplitudes is shown in the Δt distribution of fig. 4-b, where $\Delta t = |t_{\pi\pi}| - |t_{\pi f}|$ is equivalent to the Jackson angle of the π^+ in the $\pi^+ f^o$ system. The solid curve, a, is the contribution of diagram 3-a (f^o-exchange) and the solid curve, b, is the contribution of 3-b (A_2-exchange); these curves were normalized to the wings of the Δt distribution. The dashed curve, b', represents the contribution of 3-b (π-exchange) and is normalized to the same area as curve b. An incoherent sum of the solid lines provides a good description of the data; A_2 exchange is evidently more favored than π-exchange.

Arguments steming from the duality concept [4] relating s-channel and t-channel scattering amplitudes suggest that reactions in a kinematical region where both diagrams contribute strongly can be described, on the average, equally

well by either diagram. However, if the interference between the two diagrams is included, the contributions will have been improperly altered by double counting. In two-body scattering the domains of t-channel and u-channel scattering amplitudes are well separated and their application as an asymptotic approximation is essentially unambiguous. This situation does not necessarily prevail for the three body case and care must be taken in adding approximations to amplitudes in different channels. We determine the normalization constants $N(f^{o}[p])$ and $N(A_2[p])$ and avoid double counting in the sense of duality by subdividing the data sample in the Δt distribution into disjoint phase space regions as indicated by the vertical dashed line in fig. 4-b. Because both diagrams yield essentially the same results for small value of Δt , the point of partition is not critical and was chosen at a value intermediate in the overlap region of the two diagrams; this point, $\Delta t = -0.2$ $(GeV/c)^2$ roughly divides the data into equal parts.

The Δt spectrum and partition point depend upon the accepted ranges of $t_{\pi\pi}$ and $t_{\pi f}$ as well as the lower bound of $M_{\pi^+ p}$; however, the area of dominance of the two diagrams changes in a corresponding way so that the results do not depend sensitively upon the selection critera.

Events to the left of the partition in fig. 4-b, refered to as Region-I, will be described by $A(f^{o}[p])$ whereas the events in Region-II will be described by $A(A_2[p])$ or $A(\pi[p])$. Region-I and -II contain 214 and 249 events respectively.

The invariant masses of the pi-plus in the f^{o}, $(\pi^+ f^{o})$, with the proton and the pi-minus in the f^{o}, $(\pi^- f^{o})$ with the final π^+ were examined for influences of the Δ^{++} and ρ^{o} resonances respectively. In Region-I, the ρ^{o} and Δ^{++} enhancements in $M_{\pi^+\pi^- f^{o}}$ and $M_{\pi^+ f^{o}}$ were each less than 5% above a smoothly drawn curve through the data. In, Region-II, the Δ^{++} enchancement was less than 10% and there was no ρ bump.

5. Results

The c.m. longitudinal momentum distributions of the π^+ and f^o are shown separately for Regions-I and -II in fig. 5. The solid curves represent the prediction of $A(f^o[p])$ for Region-I and $A(A_2[p])$ for Region-II; the dashed curve represents $A(\pi[p])$. We observe that f^o and A_2 exchange describe the single particle distributions quite well in their respective regions; whereas π-exchange yields a poor description of the data.

Four-momentum transfers squared to the π^+ and to the f^o are given in fig. 6, where again, the solid curves represent f^o and A_2 exchanges and provide a good description of the data. The dashed curve in Region-II of the $t_{\pi f^o}$ plot corresponding to the π-exchange prediction disagrees strongly with the data.

The $\pi^+ f^o$ invariant mass distribution is shown in fig. 7 with the predictions of f^o, A_2 and π-exchanges; we again note the complete overlap and similarity of predictions of the diagrams in the $M_{\pi^+ f^o}$ spectrum characteristic of diffraction scattering. Invariant mass distributions of the $\pi^+ p$ and pf^o are shown in fig. 8 with the predictions of f^o and A_2 exchanges given by solid curves. The dashed curve corresponding to π-exchange consistently disagrees with the data. The distributions in the Toller and Treiman-Yang angles are given along with the predictions of the double-Regge model in fig. 9, the agreement is observed to be good.

The Berger amplitudes [5] were also calculated for the diagrams in fig. 3 and found to differ from the simple pole model in no significant way for the range of variables taken herein.

6. Pion Diffractive Vertex

Analysis of events in the pion diffractive catagory in carried out in terms of the single diagram 3-c. However, for this sample the surplus of events in the ρ region of $M_{\pi^-\pi^+}$ is 25% and the expected low mass peaking in the $M_{f^o p}$ distribution constrains $M_{\pi^+ f^o p}$ to the Δ^{++} mass region. The c.m. longitudinal

momentum distributions of p and f^o are given in fig. 10; the t_{pp} spectrum is shown in fig. 11 and the invariant mass distributions are given in fig. 12, along with the model predictions. The data are well described by the model, despite the large background effects.

7. Conclusion

A simple double-Regge model with two exchange diagrams provides a good description of the diffractively produced πf^o system; double counting is avoided by normalizing the data in a way consistent with duality. It is apparent from the kinematical relationship

$s_{\pi f^o} + t_{\pi\pi} + t_{\pi f^o} = 2m_\pi^2 + m_{f^o}^2 + t_{pp}$ that if peripheral mechanisms exist to allow simultaneously low-peaked spectra in $t_{\pi\pi}$, $t_{\pi f^o}$, and t_{pp}, there will result a consequent low mass peak in the πf^o effective mass; or conversely, if there is a low mass resonance in the πf^o system the meson-meson four-momentum transfers will tend to be small since the resonance can be produced diffractively. We have shown that at least part of the low mass πf^o enchancement can be effectively reproduced by the exchange diagrams of fig. 3.

It is noteworthy that the events in Region-II are described by Pomeranchuk/A_2 exchange. In constrast, the $f^o\Delta^{++}$ data is consistent with π exchange; [6];, however, the $t_{\pi f^o}$ spectra have different ranges in the two cases.

1. J. A. Gaidos, C. R. Ezell, J. W. Lamsa and R. B. Willmann, Purdue Preprint COO-1428-228, Phys. Rev. (1970).

2. J. A. Gaidos, C. R. Ezell, J. W. Lamsa and R. B. Willmann, Purdue Preprint COO-1428-231, Nuclear Physics B (1970)

3. F. James, CERN Program Library.

4. R. Dolen, D. Horn and C. Schmid, Phys. Rev. 166 1768 (1968). G. F. Chew and A. Pignotti, Phys. Rev. Letters 20, 178 (1968)

5. E. L. Berger, Phys. Rev. 166 1078 (1968)

6. To be published.

Table Captions

Table 1. Bounds of the domain to which the double-Regge model was applied.

PROTON DIFFRACTIVE	PION DIFFRACTIVE
$q_L^p < -2.0$ GeV/c	$q_L^p > -2.0$ GeV/c
$-t_{pp} < 0.5$ $(\text{GeV/c})^2$	$-t_{pp} < 0.5$ $(\text{GeV/c})^2$
$-t_{\pi\pi} < 2.0$ $(\text{GeV/c})^2$	$-t_{\pi\pi} < 1.0$ $(\text{GeV/c})^2$
$-t_{\pi f} < 2.0$ $(\text{GeV/c})^2$	$m_{\pi p} > 1.6$ GeV
$m_{\pi p} > 1.6$ GeV	

TABLE I

Figure Captions

Fig. 1. C.m. longitudinal momentum distributions. Hatching indicates those events selected as proton diffractive or pion diffractive within the ranges listed in Table I.

Fig. 2. Distributions of four-momentum transfer to the diffractive vertices.

Fig. 3. Double exchange diagrams.

Fig. 4. (a) Scatter plot of $-t_{\pi f^o}$ vs. $-t_{\bar{\pi}\pi}$. (b) Distribution in $\Delta t = |t_{\bar{\pi}\pi}| - |t_{\pi f^o}|$; the curves a, b, b' represent f^o, A_2 and π exchange, respectively.

Fig. 5. C.m. longitudinal momentum distributions; the solid curves represent the predictions of f^o and A_2 exchange for Regions-I and -II respectively; the dashed curve is the prediction of π-exchange.

Fig. 6. Spectra of four-momentum transfers; the solid lines represent model predictions, the dashed line corresponding to π exchange.

Fig. 7. Effective mass distribution of the $\pi^+ f^o$ system with curves from the double-Regge model.

Fig. 8. Effective mass distributions of the $\pi^+ p$ and $p f^o$ systems. The curves are obtained from the double-Regge model.

Fig. 9. Distributions of the Toller angles and the Treiman-Yang angles with curves from the double-Regge model.

Fig. 10. C.m. longitudinal momentum distributions of the f^o and π^+ with curves from the double-Regge model.

Fig. 11. Spectrum of t_{pp} with the predictions of the double-Regge model.

Fig. 12. Effective mass distributions of the $\pi^+ f^o$, $\pi^+ p$ and $p f^o$ systems. The curves are predictions of the double-Regge model.

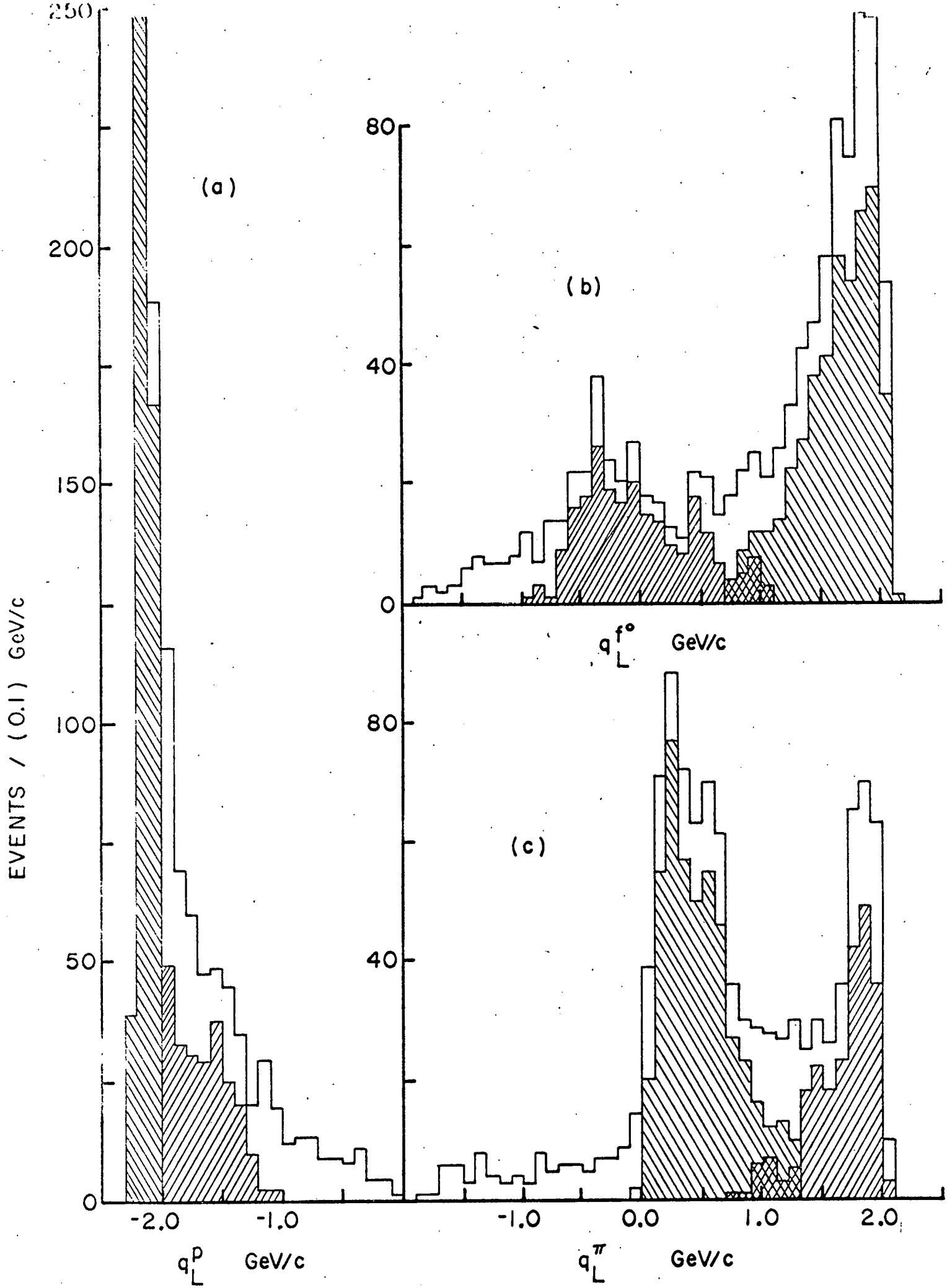
(a)
(b)
(c)
EVENTS / (0.1) GeV/c
250
200
150
100
50
0
80
40
0
80
40
-2.0
-1.0
-1.0
0.0
1.0
2.0
q_L^p GeV/c
$q_L^{f^\circ}$ GeV/c
q_L^π GeV/c

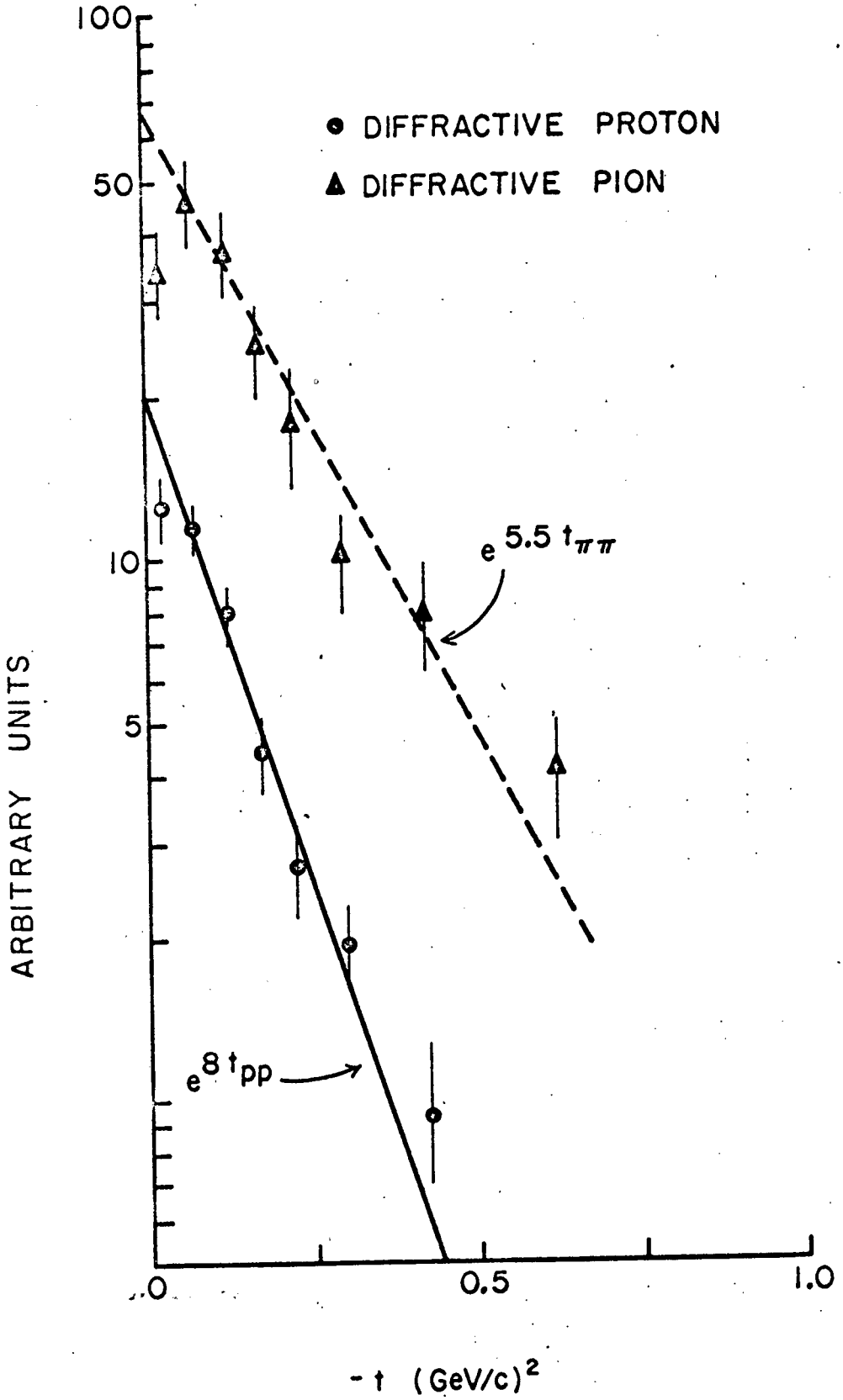
100
50
10
5
1.0
0.5
.0
DIFFRACTIVE PROTON
DIFFRACTIVE PION
$e^{5.5\,t_{\pi\pi}}$
$e^{8\,t_{pp}}$
ARBITRARY UNITS
$-t$ (GeV/c)^2

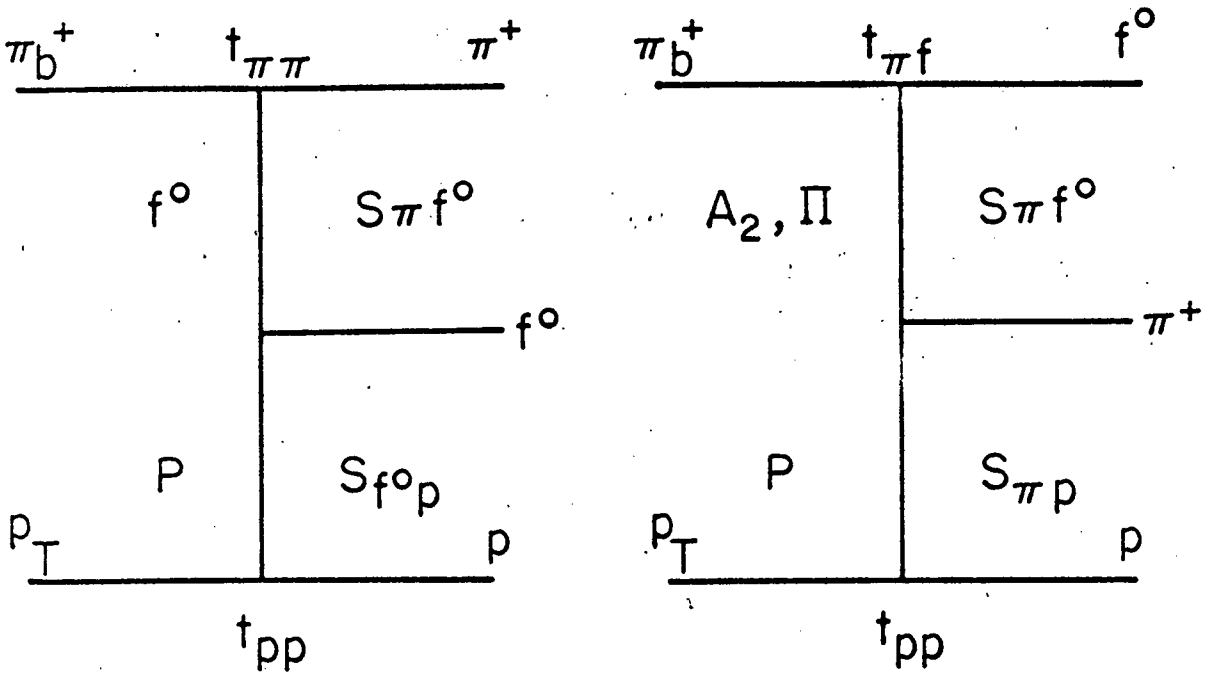
π_b^+
$t_{\pi\pi}$
π^+
f^o
$S_\pi f^o$
f^o
P
$S_{f^o p}$
p_T
p
t_{pp}
(a)
π_b^+
$t_{\pi f}$
f^o
A_2, Π
$S_\pi f^o$
π^+
P
$S_\pi p$
p_T
p
t_{pp}
(b)

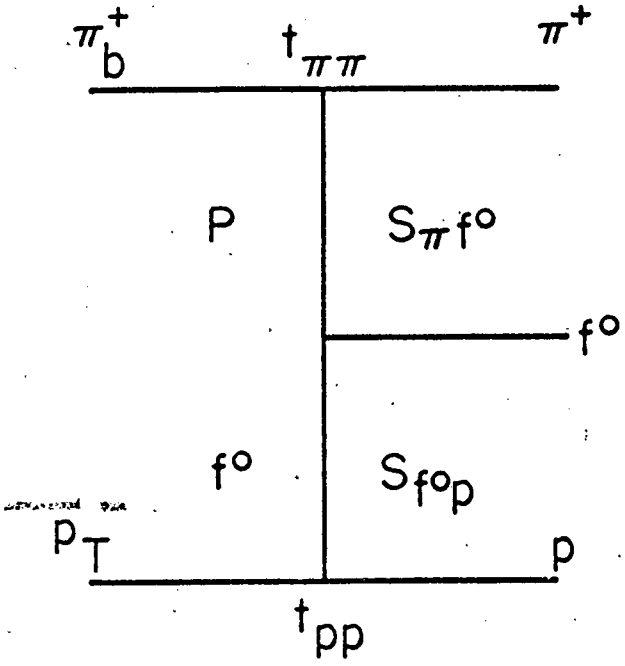
π_b^+
$t_{\pi\pi}$
π^+
P
$S_\pi f^o$
f^o
f^o
$S_{f^o p}$
p_T
p
t_{pp}
(c)

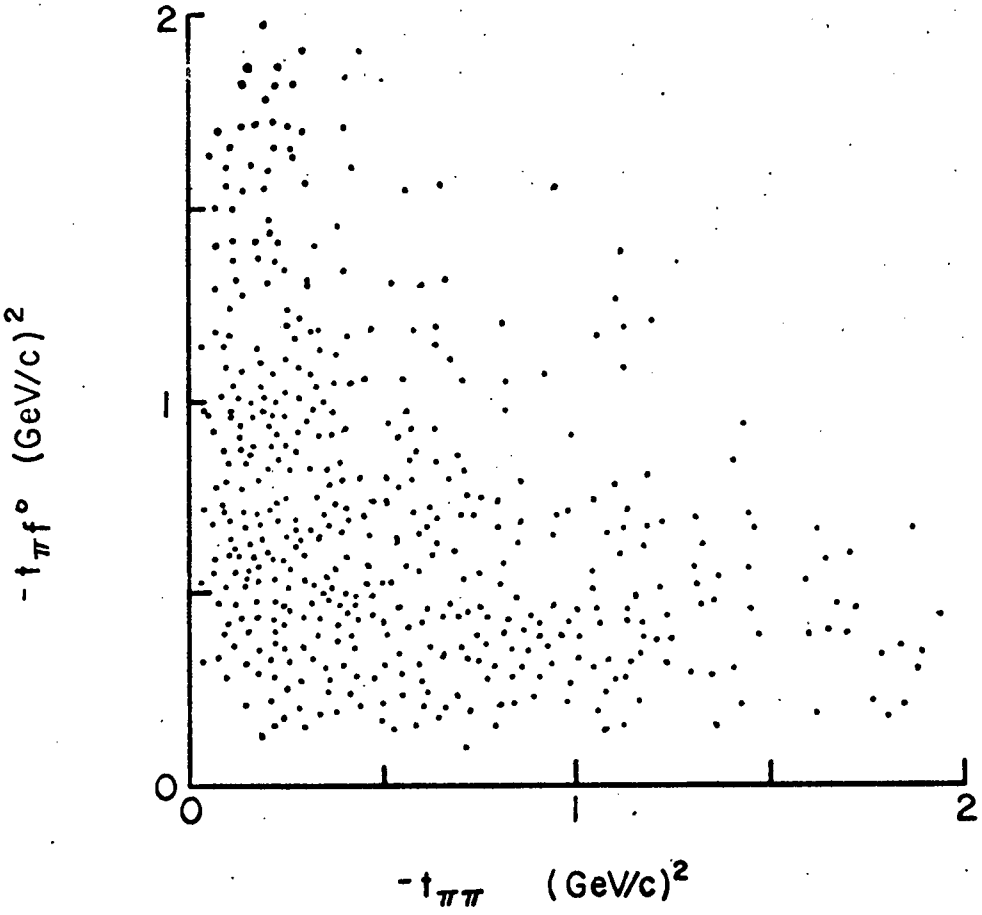
2
1
0
0
1
2
$-t_{\pi f^0}$ (GeV/c)^2
$-t_{\pi\pi}$ (GeV/c)^2

(a)

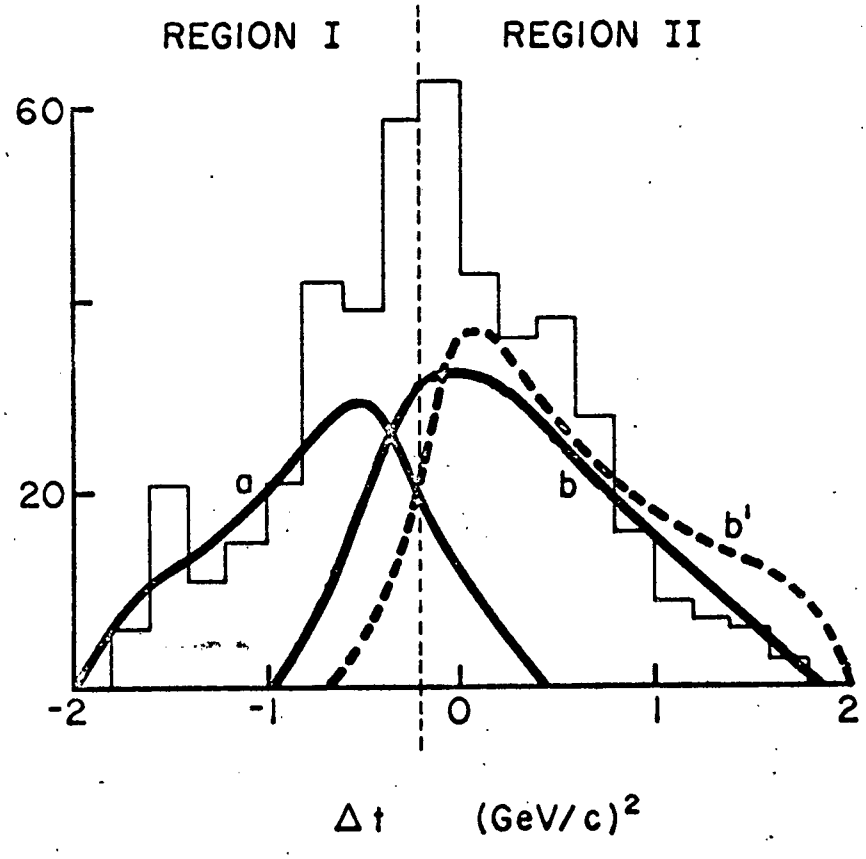
REGION I
REGION II
60
20
a
b
b'
-2
-1
0
1
2
Δt (GeV/c)^2

(b)

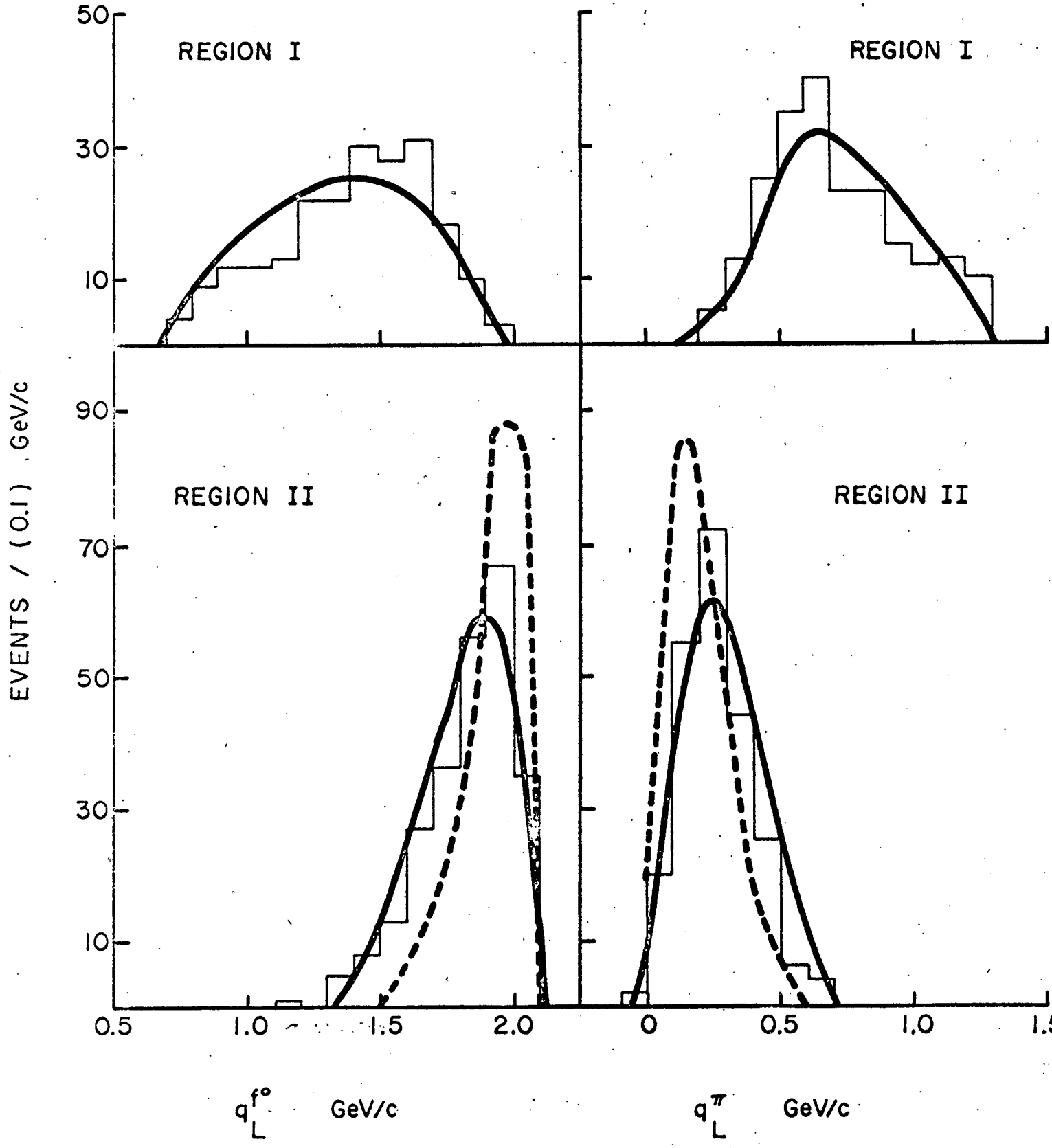
REGION I
REGION I
REGION II
REGION II
50
30
10
90
70
50
30
10
EVENTS / (0.1) GeV/c
0.5
1.0
1.5
2.0
0
0.5
1.0
1.5
$q_L^{f^\circ}$ GeV/c
q_L^{π} GeV/c

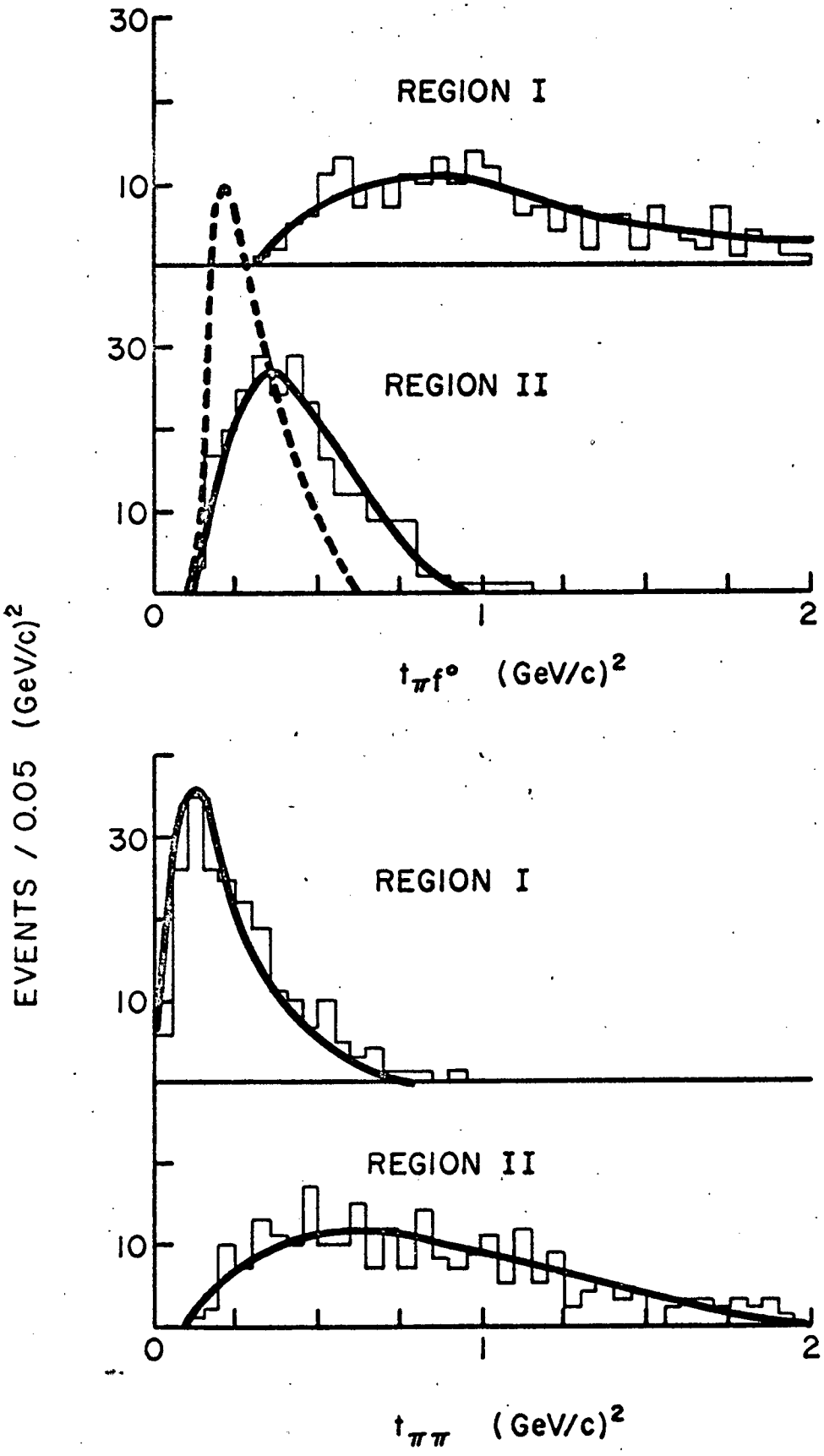
REGION I
REGION II
30
10
30
10
0
1
2
$t_{\pi f^0}$ (GeV/c)^2
EVENTS / 0.05 (GeV/c)^2
REGION I
REGION II
30
10
10
0
1
2
$t_{\pi\pi}$ (GeV/c)^2

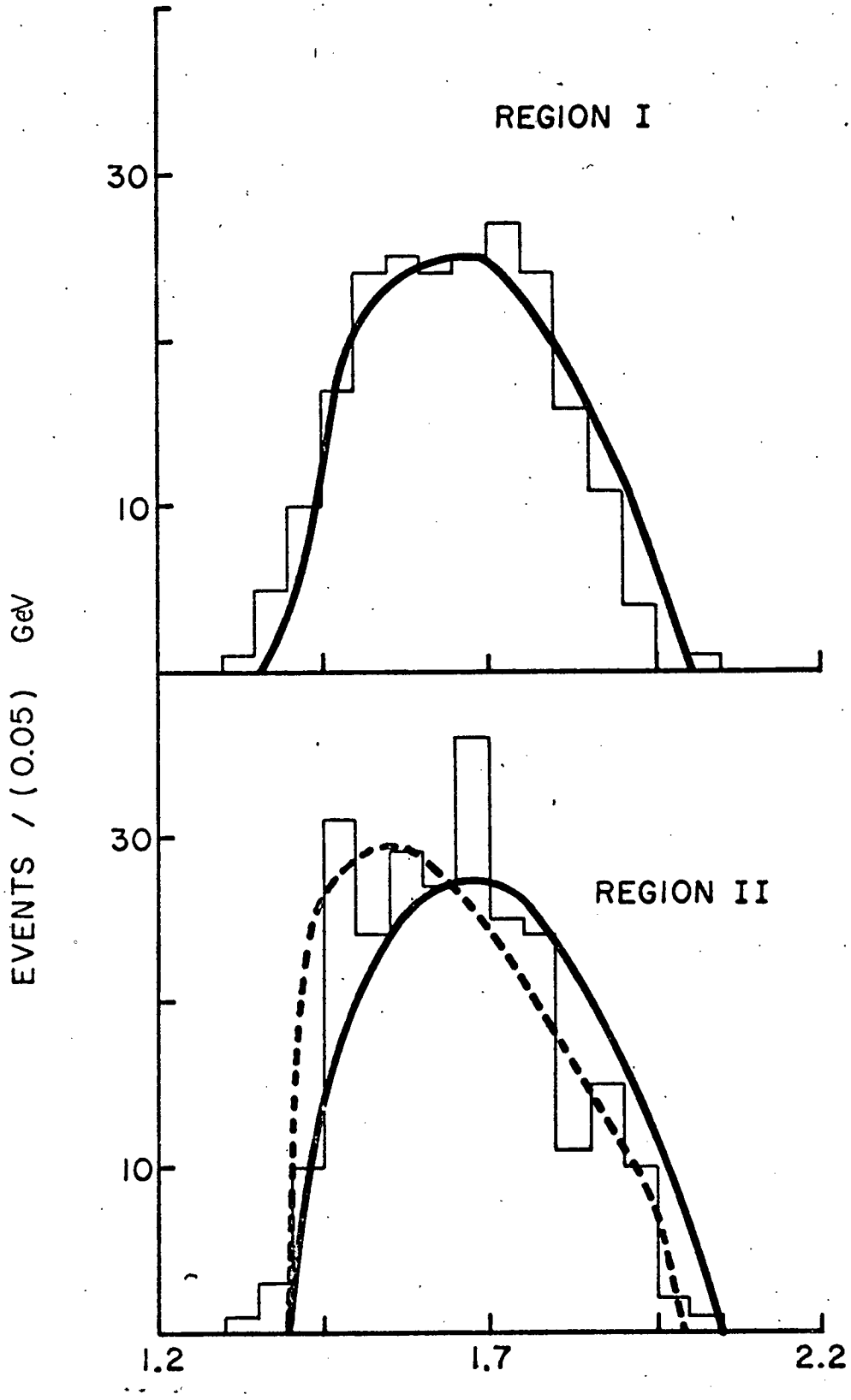
REGION I
30
10
REGION II
30
10
EVENTS / (0.05) GeV
1.2
1.7
2.2
$M_{\pi^+ f^0}$ GeV

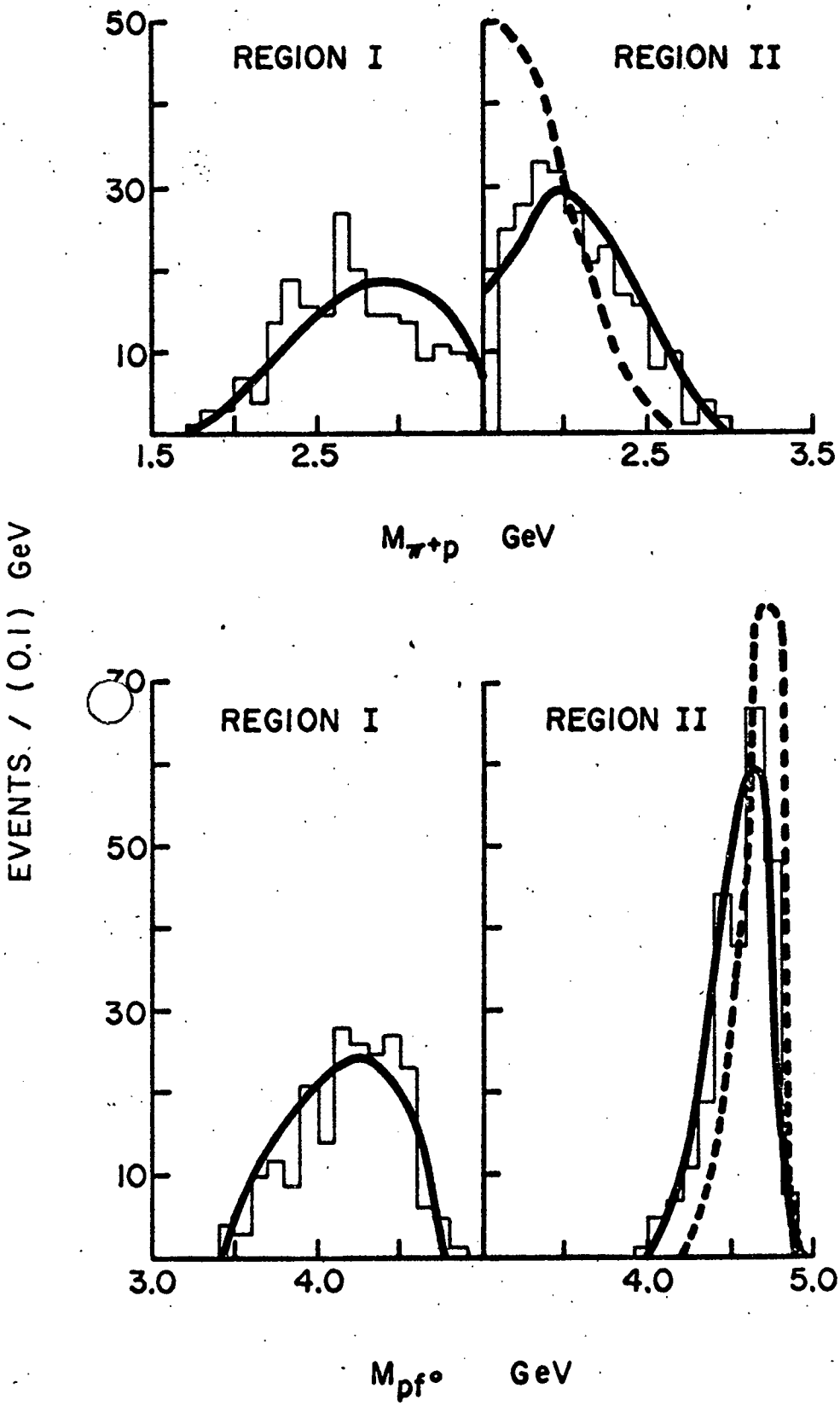
50
30
10
REGION I
REGION II
1.5
2.5
2.5
3.5
M_{π^+p} GeV
EVENTS / (0.1) GeV
70
50
30
10
REGION I
REGION II
3.0
4.0
4.0
5.0
M_{pf° GeV

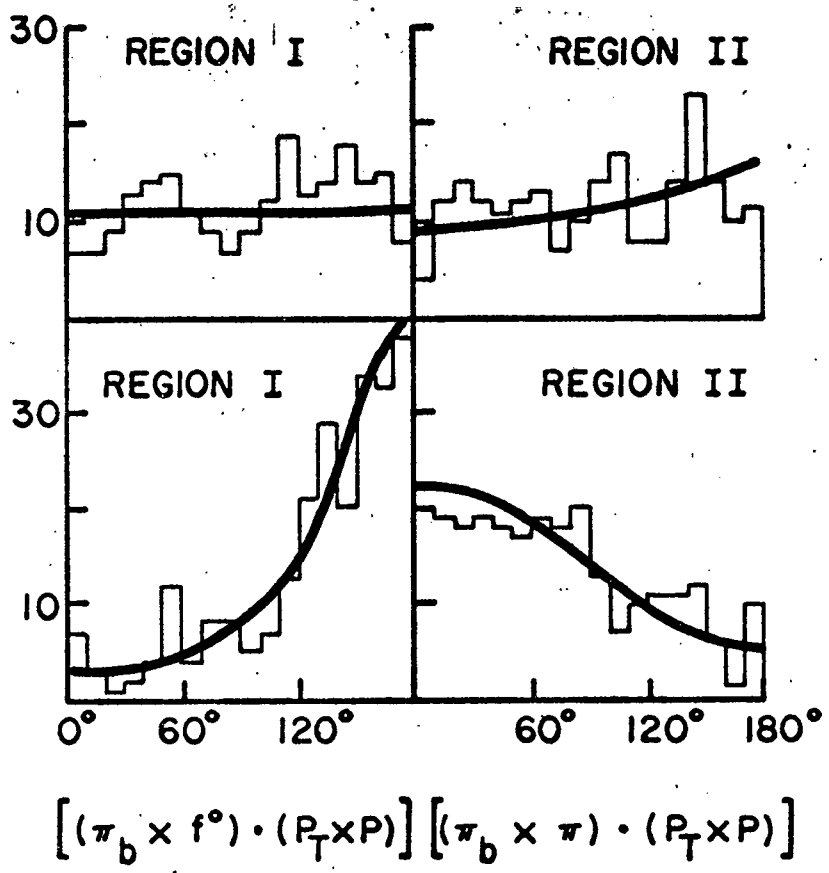

EVENTS / 10°

$[(\pi_b \times f^\circ) \cdot (P_T \times P)]\,[(\pi_b \times \pi) \cdot (P_T \times P)]$

π^+ c.m.s. f° c.m.s.

TOLLER ANGLE

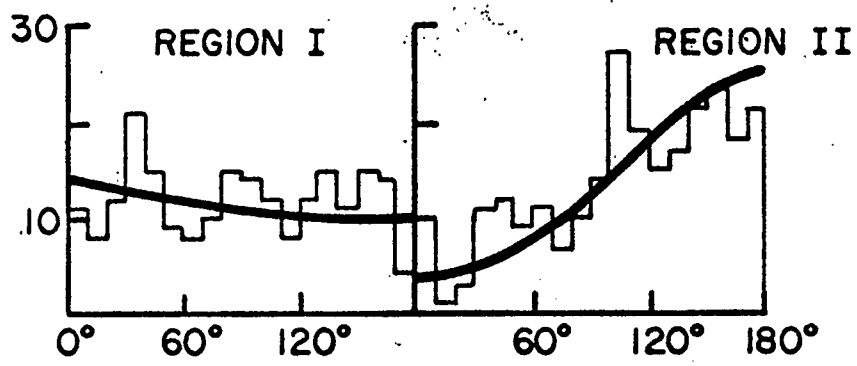

$(\pi_b \times \pi) \cdot (P \times P_T)$

$\pi^+ f^\circ$ c.m.s.

TREIMAN — YANG ANGLE

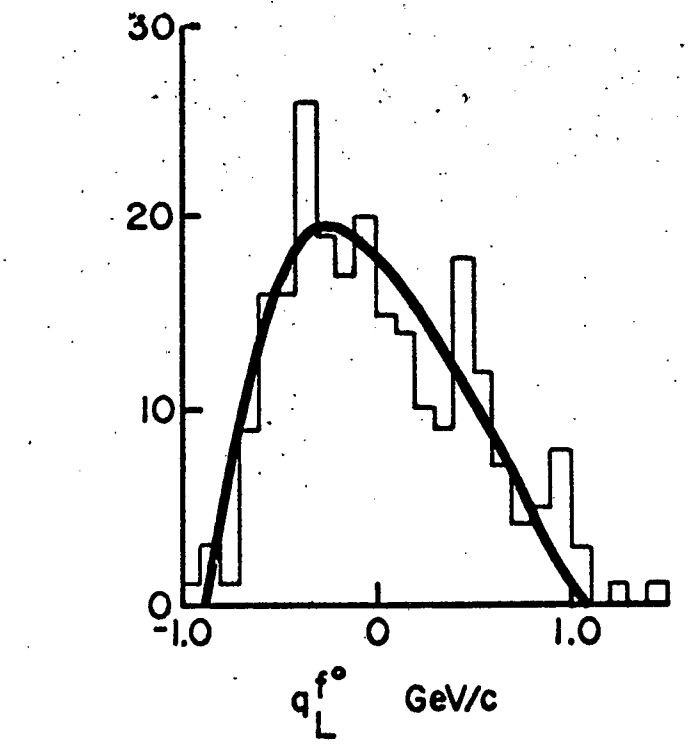
30
20
10
0
-1.0
0
1.0
$q_L^{f^\circ}$ GeV/c

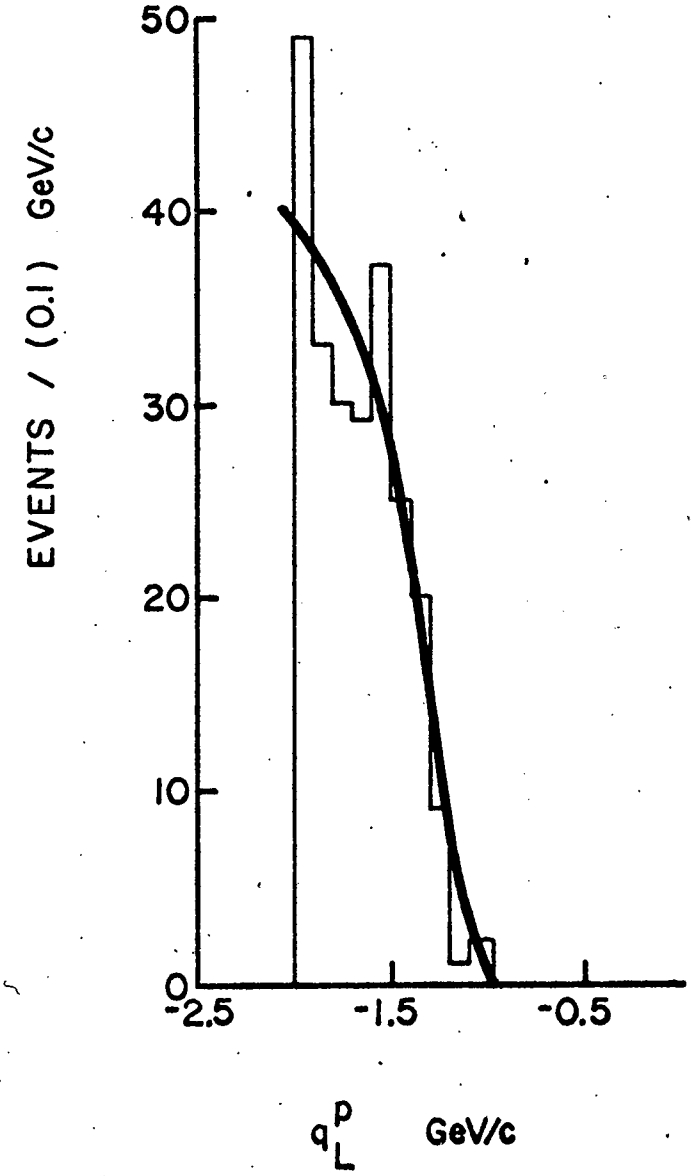
EVENTS / (0.1) GeV/c
50
40
30
20
10
0
-2.5
-1.5
-0.5
q_L^p GeV/c

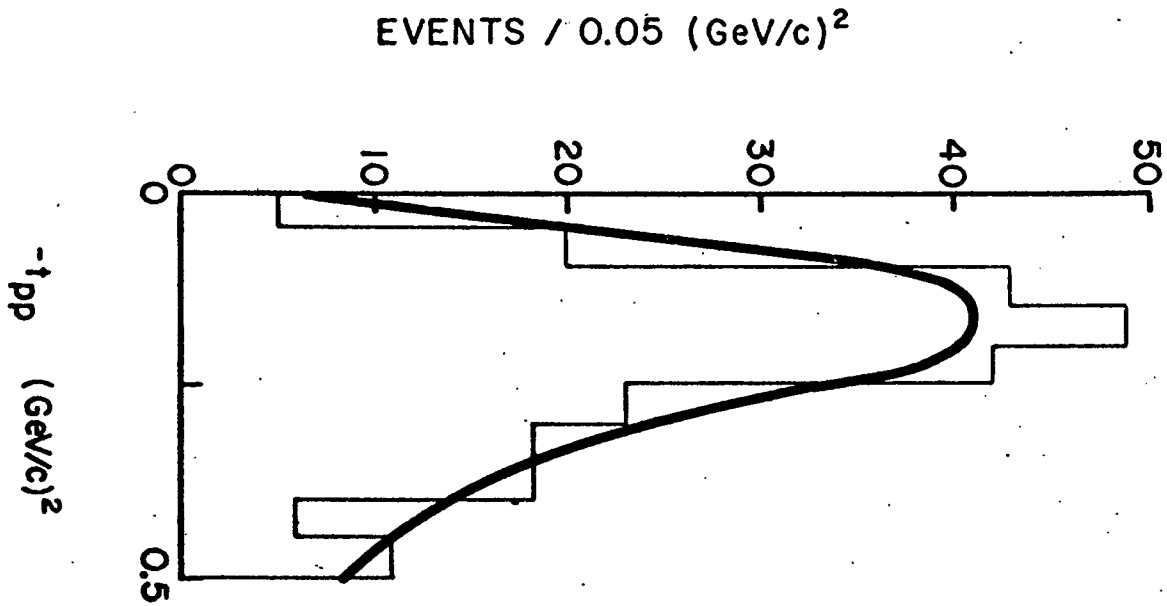
EVENTS / 0.05 (GeV/c)²
0
10
20
30
40
50
0
0.5
-t_pp (GeV/c)²

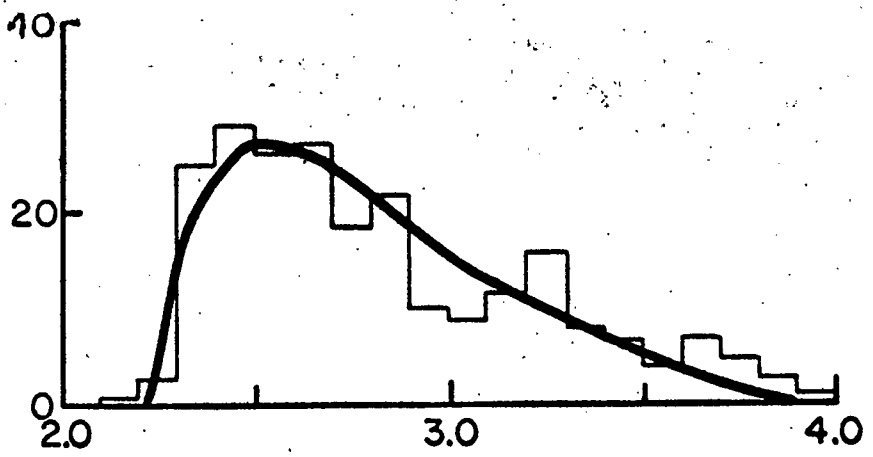

M_{pf° GeV

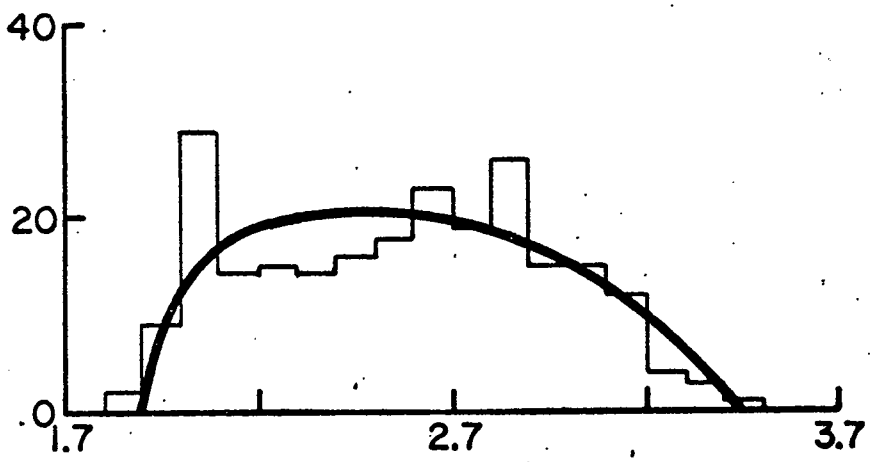

$M_{\pi^+ f^\circ}$ GeV

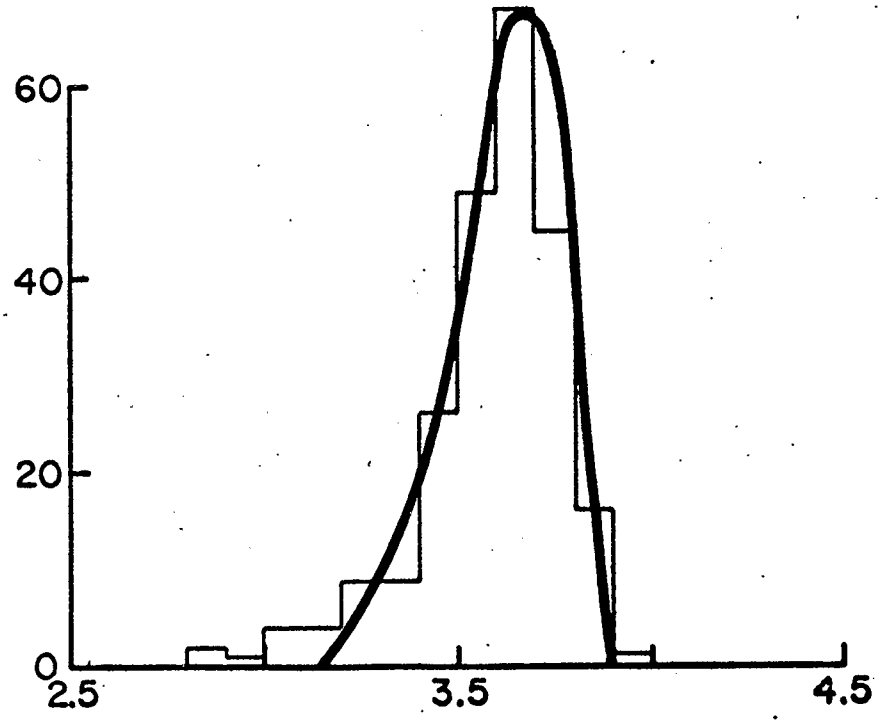

$M_{\pi^+ p}$ GeV